



Cite this: *J. Mater. Chem. C*, 2016,  
4, 4040

## On the impact of isomer structure and packing disorder in thienoacene organic semiconductors†

Karl J. Thorley and Chad Risko\*

Many high performing organic semiconductor materials contain heteroaromatic rings in order to control the molecular packing and material electronic properties. Here we use a combination of density functional theory and symmetry-adapted perturbation theory calculations to explore the intermolecular noncovalent interactions, which guide solid-state molecular packing, and electronic couplings in a series of benzodithiophene-based dimer models. A novel concept, termed the disordermer, is introduced to delineate how the reduced molecular symmetry of benzodithiophene, when compared to the more highly symmetric anthracene molecule, can present intermolecular isomerism in the solid state that results in a wide range of available molecular packing arrangements that in turn influence the magnitudes of the electronic couplings. The insight developed through the investigation of these disordermers is demonstrated to hold important implications in the design of new generations of organic semiconductor materials.

Received 20th November 2015,  
Accepted 11th March 2016

DOI: 10.1039/c5tc03900b

www.rsc.org/MaterialsC

### Introduction

With the promise to manufacture low power flexible devices through simple printing techniques, the field of organic electronics continues to garner much academic and commercial interest. Polycyclic aromatic hydrocarbon molecules are at the heart of many organic semiconductor (OSC) materials, with heteroatoms often incorporated into the  $\pi$ -conjugated backbone to optimize the (isolated) molecular electronic properties and influence the intermolecular interactions and charge-carrier transport characteristics of the solid-state material.<sup>1–3</sup> Thiophene continues to be among the main heterocycles employed in materials design, finding broad application in molecular and polymeric materials for field-effect transistors<sup>4–7</sup> and organic solar cells.<sup>8–11</sup>

The thiophene motif has been incorporated into acene structures in a wide variety of configurations. Among the more successful molecular materials for field-effect transistor applications are anthradithiophene (ADT) and benzo[thienobenzothienophene] (BTBT). ADT, where thiophene rings are fused to the exterior of an anthracene core (and often include the silylethynyl functionalization approach of Anthony<sup>5,12</sup> appended to the center of the molecule), has been widely used as a thin-film molecular material that presents relatively large hole mobilities (up to  $6 \text{ cm}^2 \text{ V}^{-1} \text{ s}^{-1}$ ) extracted from field-effect transistor measurements.<sup>13</sup> BTBT, on the other hand, features internally fused thiophene rings capped with benzene rings,

and terminal alkyl chains for solubility.<sup>14</sup> Inkjet-printed crystals of dioctyl BTBT are champion materials, leading to some of the largest transistor hole mobilities measured for an organic semiconductor (up to  $30 \text{ cm}^2 \text{ V}^{-1} \text{ s}^{-1}$ , with an average of  $16 \text{ cm}^2 \text{ V}^{-1} \text{ s}^{-1}$  across a range of devices).<sup>15</sup>

In general, it is assumed that the large, diffuse, electron rich sulfur atoms provide good electronic communication with neighboring molecules, leading to increased electronic coupling relative to their carbon analogs. Less well understood is the impact of the sulfur atoms on the nature of the intermolecular interactions that ultimately impact the molecular packing configurations. These determine, in large part, the overlap of the wave functions of the neighboring molecules and, in turn, the intermolecular electronic coupling, a critical component of the charge-carrier transport efficiency. Wheeler,<sup>16</sup> Sherrill,<sup>17,18</sup> Tsuzuki,<sup>19</sup> and others have explicitly considered how the chemical makeup of heteroatoms in small aromatic systems impact the nature and strength of noncovalent intermolecular interactions (*i.e.* exchange-repulsion, dispersion, electrostatics, and induction), and demonstrated how these interactions lead to the energetically preferred molecular packing configurations in model dimers, though studies on device-relevant molecules remain limited.

As molecular organic semiconductor materials generally take (poly)crystalline forms in the solid state, pathways of consistent molecular alignments that mitigate the presence of traps are necessary to provide the prominent charge-carrier transport conduits through the active layer. From a materials design standpoint, it is important to realize that the inclusion of thiophene into an acene structure can lead to an isomeric

Department of Chemistry & Center for Applied Energy Research, University of Kentucky, Lexington, Kentucky 40506-0055, USA. E-mail: chad.risko@uky.edu

† Electronic supplementary information (ESI) available. See DOI: 10.1039/c5tc03900b

mixture of products, which has led to a number of recent efforts to understand how isomeric purity impacts material characteristics. For instance, isomerically pure bis triethylsilyl *syn* difluoro-anthradithiophene (diF-ADT) was synthesized by Tykewski and co-workers, with the resulting thin-film transistors presenting comparable performance to devices with the active layer prepared from a mixture of *syn* and *anti* isomers.<sup>20</sup> Chromatographic separation of key synthetic intermediates can allow for the isolation of both *syn* and *anti* silylethynyl diF-ADTs in pure form,<sup>21</sup> and similar transistor performance was shown for materials derived from the *syn* and mixed ADTs, though the pure *anti* isomer presented a larger transistor hole mobility. Similar trends have been observed in unfunctionalized ADTs.<sup>22,23</sup>

In addition to isomeric purity, one should also consider the impact of the molecular symmetry. Particularly for molecules with low degrees of symmetry, it is possible for adjacent molecules to pack in a disordered manner despite the molecules being isomerically equivalent. For the isomerically pure ADTs, the *anti* isomer shows the lowest degree of thiophene positional disorder in the experimental crystal structures,<sup>21,23</sup> which could lead to more homogenous charge-carrier transport pathways, offering a plausible explanation for the larger hole mobilities determined from transistor studies.

Here we are interested in detailing the impact of such disorder by describing the intermolecular noncovalent interactions that direct solid-state molecular packing and the resulting electronic couplings, a key parameter that can be used to gauge charge-carrier transport characteristics, for a series of thienoacene dimers. To discuss the effects of disorder in a more descriptive manner, we introduce the concept of the disordermer – a form of intermolecular dissimilarity between regiochemically identical molecules due to disorder in the crystalline state – to take into account that identical, isomerically pure molecules in a crystalline environment can interact with each other in different ways depending on the symmetry of the single molecules. In solution, these molecules are identical due their averaged molecular motion, but in the solid state the position of the molecule is fixed by the surrounding molecules, and it is no longer possible to convert between disordermers (Fig. 1).

To describe disordermers in crystal structures, we can consider two transformations. The first transformation describes how the position of one molecule in a crystal is related to the position of its neighbors, and can consist of a three dimensional

translation and/or molecular rotation. The transformation can be specified through the use of a Cartesian coordinate system defined from the center of the molecule, or through crystallographic axes and fractional coordinates. This transformation is (ideally) unchanged by the inclusion of disorder. The second transformation applies to individual molecules,<sup>24</sup> with operations similar to those used to define point groups that induce the disordered structures. We concentrate here on the Schoenflies notation for point group transformations. These operations are applied based on the point group of the molecule, where the principal rotation axis is defined as the z-axis. Applying an operation belonging to the point group will give the same disordermer structure, while applying a related transformation not associated with the point group will result in an alternate disordermer. This transformation should be of the same order as a valid symmetry operation to preserve the overall packing structure, e.g. a  $C_2$  rotation around a different axis in a  $C_{2v}$  molecule. To differentiate between the transformations, we will use xyz axis labels based on the point group of the molecule for those transformations operating on a single molecule to induce disorder, and Cartesian ABC axis labels for those that describe the relationship between adjacent molecules.

In the present study, we construct disordermer pairs to investigate the intermolecular noncovalent interactions and electronic couplings of benzodithiophene (BDT), a molecular moiety often used in oligomeric and polymeric organic materials due to its rigid construction and facile chemical functionalization. As a smaller analog of ADT, BDT offers the possibility to readily investigate the effects of isomerism of the *syn* and *anti* isomers. Thus, our current study using BDT will have direct impact on the ongoing studies involving isomeric purity and disorder in larger heteroacenes and oligomeric materials.

## Computational details

Molecular geometries were optimized at the B3LYP/6-31G(d)<sup>25,26</sup> level of theory using the Gaussian09 (Revision A.02) software suite.<sup>27</sup> Electronic couplings for both holes (HOMO:HOMO) and electrons (LUMO:LUMO) were evaluated using the fragment orbital approach.<sup>28,29</sup> The magnitude of the intermolecular noncovalent interaction energies were determined with symmetry adapted perturbation theory (SAPT)<sup>30,31</sup> with the jun-cc-pVDZ<sup>32,33</sup> basis set using the Psi4 package.<sup>34</sup> In particular, we made use of the SAPT0 approximation, which neglects the intramolecular correlation: when used in combination with the truncated diffuse jun-cc-pVDZ basis set, the resulting interaction energies are comparable to higher level calculations<sup>35</sup> at much reduced computational time; for simplicity, results arising from the SAPT0/jun-cc-pVDZ calculations will be referred to as SAPT0. In addition to providing accurate values for interaction energies ( $E_{\text{int}}$ ), this method allows for the decomposition of the noncovalent interactions into exchange ( $E_{\text{exch}}$ ), electrostatic ( $E_{\text{elec}}$ ), induction ( $E_{\text{ind}}$ ) and dispersion ( $E_{\text{disp}}$ ) terms, allowing us to pinpoint the stabilizing or destabilizing contributions in each molecular pair. Note that these

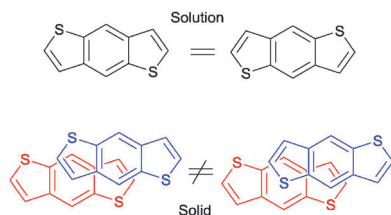


**Fig. 1** Schematic description of the disordermer. In solution, the top structures are equivalent due to their averaged molecular motion. In the solid state, the molecular positions are fixed, so the blue molecule cannot reorient with respect to the red molecule. In this case, there are two possible disordermers.

component terms sum to the total interaction energy, as shown in eqn (1):

$$E_{\text{int}} = E_{\text{exch}} + E_{\text{elec}} + E_{\text{ind}} + E_{\text{disp}} \quad (1)$$

## Results and discussion

### Setting up the disordermers

To begin, we will establish essential differences in the structure of three molecules: anthracene, *anti*-BDT, and *syn*-BDT. Anthracene belongs to the highly symmetric  $D_{2h}$  point group (*mmm* by the Hermann–Mauguin notation), which removes any possibility for isomeric impurity and corresponding intermolecular disorder. The *anti* and *syn* isomers of BDT, depicted in Fig. 2, have  $C_{2h}$  ( $2/m$ ) and  $C_{2v}$  ( $mm2$ ) symmetry, respectively. This means that BDT (in dimer models or the solid state) can be “disordered” by some of the symmetry operators from the  $D_{2h}$  point group. For example, rotation of *anti* BDT around either the  $x$  or  $y$  axes results in a change in the position of the thiophene ring atoms, though the central benzene ring atoms remain unchanged. These operations do not appear in the definition of the point group for each molecule, but are closely related. The transformations resulting in disorder for *anti* and *syn* BDT are summarized in Fig. 2. In experimental crystal structures, there will usually be one major disordermer with higher occupancy. This can be referred to as the  $E$  disordermer, in reference to the identity operator. Here, we arbitrarily assign the  $E$  disordermer to the depiction given in Fig. 2. Other possible disordermers can

be named after the symmetry operation required to generate it (e.g.  $C_2(x)$ ), although there may be more than one operation that results in the same structure. The molecular properties of the two BDT isomers are similar, with the molecular orbital eigenvalues very close to each other. Due to the inversion center, *anti*-BDT does not have a permanent dipole moment, though the *syn* isomer has permanent dipole moment of 1.52 D at the B3LYP/6-31G(d) level of theory. From this point forward, we focus our discussion of the noncovalent interactions and electronic couplings on BDT isomers, as the rather significant differences in atom and electron count with respect to anthracene do not allow for direct comparisons; some pertinent data related to anthracene may be found in the ESI.†

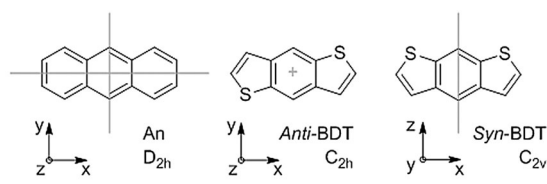
### Effect of intermolecular separation ( $C$ -displacement)

Let us first consider the impact of the intermolecular separation/vertical displacement of perfectly co-facial, “ $\pi$ -stacked” molecules. To set the models, the center of mass of one molecule is placed at the origin, and a second molecule is duplicated at varying distances in the  $C$ -direction (Fig. 3). At each new  $C$  position over the range of 3 to 5 Å, the total SAPT0 interaction energy  $E_{\text{int}}$  is determined. This process was repeated for each BDT molecule featuring ordered and disordered alignments by applying a  $C_2(x)$  rotation to the top (blue) BDT molecule (**1a**–**1d**, Fig. 3). Notably, there is no difference among the *anti* and *syn* isomers of BDT. The total intermolecular interaction energies, including the component energies from eqn (1), for molecular pairs **1a** (*anti*) and **1c** (*syn*) are identical at each  $C$ -separation, as are those for pairs **1b** (*anti*) and **1d** (*syn*).

There are, however, important differences among the ordered and disordered pairs. For the *anti* isomer, the overall SAPT0 interaction energy of disordermer pair **1a** is more stabilizing than the perfectly cofacial pair **1b** at each  $C$ -separation. This leads to an energetic minimum at a vertical intermolecular distance of 3.7 Å for **1a**, compared to 3.8 Å for **1b**. At these displacements, the invocation of disorder leads to a stabilization of 1.6 kcal mol<sup>−1</sup>.

These results suggest that the single molecule properties, including the permanent dipole in the *syn* isomer, do not influence the close  $\pi$ -stacking interactions in BDT. To uncover these relationships among molecular structure, disorder, and the intermolecular interaction energies, we compare the data sets for the *anti* BDT dimers (**1a** and **1b**, Fig. 3 right). At large distances (>4 Å), the major difference between the disordermer pairs is indeed due to electrostatic interactions (as expected), whose energies are slightly more repulsive in the disordered state **1a**. At closer distances, such as those typically found in  $\pi$ -stacked materials (3.2–3.8 Å), the major difference between the disordermer pairs is the exchange repulsion, which is stronger in the ordered pair **1b**.

These observations can be clarified by comparing the molecular structures of the *syn* and *anti* isomers in each disordermer combination, though it remains non-trivial to deconvolute the exact atomic or molecular contributions to these interactions. In the  $E$ - $E$  pairs **1b** and **1d**, there is direct overlap of the thiophene moieties in both *syn* and *anti* isomers, while applying the  $C_2(x)$  rotation to one of the molecules leads to a staggered



	An	<i>Anti</i> -BDT	<i>Syn</i> -BDT
Point Group	$D_{2h}$	$C_{2h}$	$C_{2v}$
$C_2(x)$	1	−1	−1
$C_2(y)$	1	−1	−1
$C_2(z)$	1	1	1
$i$	1	1	−1
$\sigma_h(xy)$	1	1	−1
$\sigma_v(yz)$	1	−1	1
$\sigma_v(xz)$	1	−1	1

Fig. 2 Chemical structures of the three molecules studied, with highlighted axes of rotation, centers of inversion, and planes of symmetry. The Cartesian axes shown define the axes used for transformations based on symmetry operators. The point group and symmetry operator information for the molecules are also presented. A value of 1 describes a superimposable transformation product, while −1 indicates a “disordered” product.

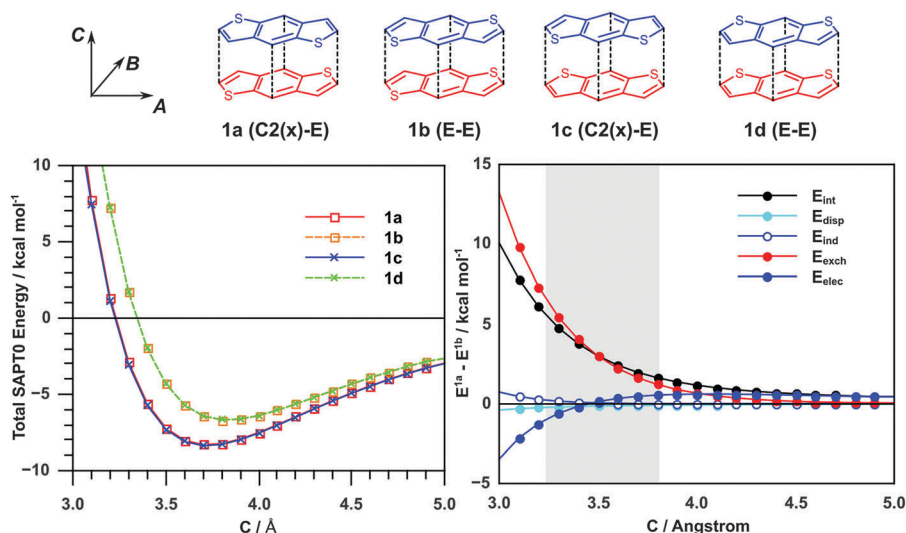


Fig. 3 (left) Total SAPT0/jun-cc-pVDZ interaction energies for *anti*-BDT and *syn*-BDT (accounting for disorder) as a function of the plane-to-plane *C*-distance. (right) Difference in the component SAPT0/jun-cc-pVDZ energies for disordermer pairs ( $E^{1a} - E^{1b}$ ) as a function of *C*-displacement. The region relevant to organic semiconductors lying between 3.2 to 3.8 Å is highlighted.

orientation of the sulfur atoms in the dimer. Thus, the isomeric identity does not affect the interaction energy but the state of disorder does, with the major destabilization of the *E-E* structure being the increased exchange repulsion interactions that arise in part from the direct overlap of the electron-rich sulfur atoms.

The intermolecular electronic couplings (*i.e.* transfer integrals) were determined as a function of the plane-to-plane *C*-displacements (Fig. 4). In general, the hole electronic couplings,  $t_h$ , determined among the highest occupied molecular orbitals (HOMO) of adjacent molecules, are quite similar across this series. At short distances, the *E-E* alignments yield larger  $t_h$  due to the direct overlap of molecular orbitals involving the diffuse sulfur atoms. Likewise, the disorder and isomeric purity do not dramatically change the electronic couplings for electrons,  $t_e$ , determined among the lowest unoccupied molecular orbitals (LUMO) of the dimers. The exception is *anti*-BDT pair 1a, which is a direct consequence of the LUMO distribution (see the ESI† for pictorial representations of the HOMO and LUMO): when the *anti* isomer stacks in a disordered fashion, there is less wave function overlap between the LUMOs, leading to smaller electronic coupling. The LUMO of *syn* BDT appears to be slightly more delocalized, and therefore does not suffer a loss of electronic coupling to the same degree upon disorder.

### Effect of long-axis (*A*) translation

So far we have only considered molecules in stacked arrangements that align the molecular centers-of-mass, which, though highly desirable as it ensures maximal wave function overlap and electronic coupling, is an arrangement not typically found in organic semiconductor materials due to the large exchange repulsion forces.<sup>1,36</sup> To establish insight into more representative solid-state arrangements, we constructed a molecular pair that is separated by 3.5 Å in the *C*-direction with parallel alignment, and then translated one of the molecules along

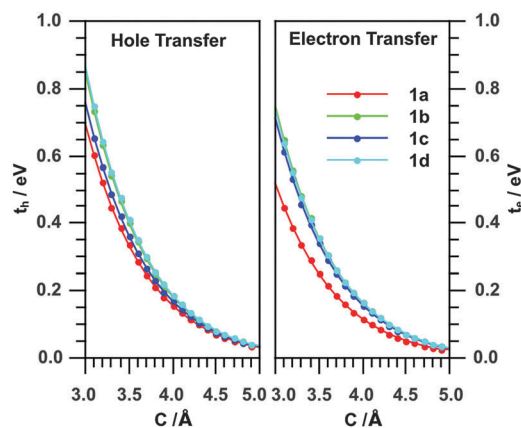


Fig. 4 Transfer integrals for holes ( $t_h$ , left) and electrons ( $t_e$ , right) for *anti*-BDT and *syn*-BDT as a function of intermolecular separation, accounting for disorder, as determined at the B3LYP/6-31G(d) level of theory.

the *A* (long)-axis. The total SAPT0 interaction energy for the BDT dimers (Fig. 5, middle, black circles) is strongest for displacements of around 1.5 Å. Looking at the noncovalent interaction energies, the dispersion force weakens with increasing *A*-axis displacement in a smooth fashion, as does the negligible induction term. The electrostatic term has some finer features with slight bumps in the curve. Major similarities are observed between the behavior of the exchange energy  $E_{\text{exch}}$  and the total interaction energy  $E_{\text{int}}$ , with the oscillations due to the local electron densities mirrored in the energy trends. At displacements smaller than 2 Å, the exchange term is more repulsive for 2a (blue filled circles) than 2b (blue open circles), leading to a smaller total SAPT0 interaction energy. Between 4 and 6 Å, the opposite is true, with a stronger exchange energy in 2b than in 2a, and thus a weaker interaction energy. Notably, these differences in the exchange and total interaction energies occur



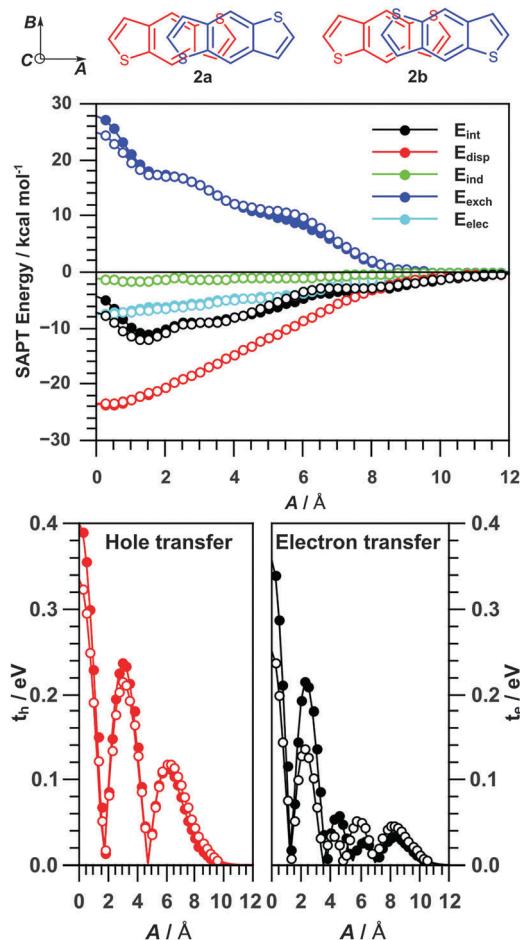


Fig. 5 SAPT0/jun-cc-pVDZ energies (top) and B3LYP/6-31G(d)-determined electronic couplings (bottom) for ordered (**2a**, solid circles) and disordered (**2b**, open circles) *anti*-BDT as a function of *A* displacement.

when thiophene moieties in the disordermer pairs interact directly with each other, rather than with the central benzene ring.

Electronic couplings determined for these molecular arrangements show that the  $t_h$  are very similar for both BDT pairs, with the *E-E* structure **2a** possessing slightly larger electronic coupling values at small *A*-axis displacements. For example, at an *A* displacement of 3 Å,  $t_h$  for **2a** is 0.23 eV compared to 0.21 eV for **2b**. At larger displacements, molecular pair **2b** presents slightly larger  $t_h$ , coinciding with the structural overlap described above.  $t_e$  yields a stronger disordermer dependence, with the ordered arrangement **2a** being more favorable for larger electronic couplings at small displacements: at 3 Å displacement,  $t_e$  is twice as large for **2a** than **2b** (0.14 eV and 0.068 eV respectively). The trends vary substantially at larger displacements due to differences in nodal positions upon the induced disorder,<sup>37,38</sup> with the electronic coupling of **2a** half the value of **2b** at 6 Å (0.051 eV *versus* 0.027 eV).

### Combining short-*(B)* and long-axis (*A*) translations

Now that we have developed a picture of how the noncovalent interactions and electronic couplings change with long-axis

displacement, we now consider short (*B*)-axis translations, as one often finds a combination of these two shifts in crystal packing motifs; we note that these shifts are presented here for the disordermer pairs of *anti*-BDT to represent the BDT family. To analyze the rather extensive set of data collected, we use both 3D surfaces and contour maps, where each line represents points of identical value. Coupling the *A*- and *B*-axis translations leads to myriad interactions: for any given *A*, *B*, *C* transformation, each molecule can occur as the *E* or *C*<sub>2</sub>(*x*) disordermer, for a total of four combinations, two of which are equivalent [*E*-*C*<sub>2</sub>(*x*) and *C*<sub>2</sub>(*x*)-*E*].

The SAPT0 energy surface for the *E-E* disordermer pair **3a** is shown in Fig. 6. Notably, the global minimum (for these albeit unrelaxed structures) occurs when the BDT molecules are offset by about 1 Å in both *A* and *B* directions. This coincides with a marked decrease in exchange repulsion due to smaller molecular overlap. Overall, the trends of the noncovalent interaction components are similar to those derived for the one-dimensional *A* displacement. The dispersion energy drops off uniformly with decreasing spatial overlap, while the induction and electrostatic contributions remain relatively small throughout (as expected). The exchange energy is distorted by local electron densities in the BDT molecules, giving rise to the uneven surfaces in both the exchange and total interaction energies with respect to the spatial overlap of the dimers.

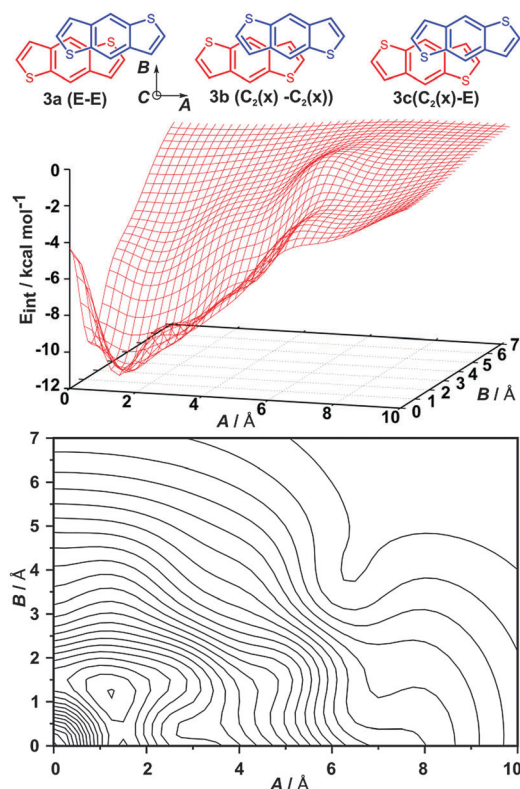


Fig. 6 SAPT0/jun-cc-pVDZ interaction energy of **3a** as a function of *A* and *B* translation in surface and contour views. The *C* separation is constant at 3.5 Å. Contours represent a change in  $E_{\text{int}} = 0.5$  kcal mol<sup>-1</sup>. Equivalent plots for disordermer pairs **3b** and **3c** are provided in the ESI.†

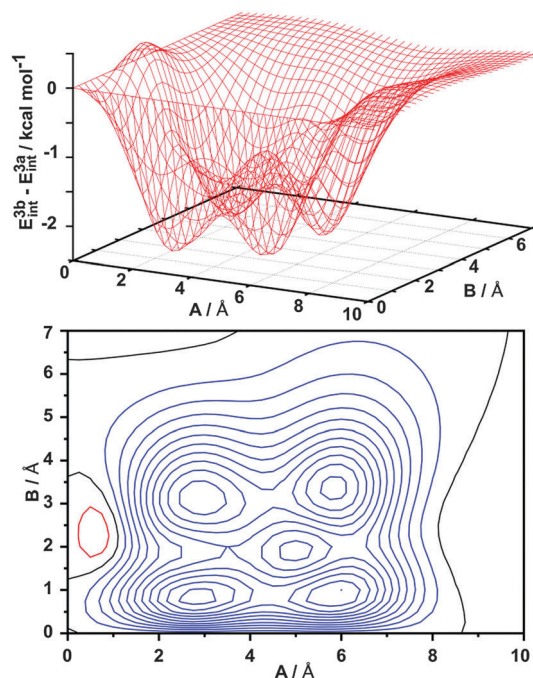


Fig. 7 Difference in SAPT0/jun-cc-pVDZ interaction energy of disordermer pairs **3b** and **3a** as a function of  $A$  and  $B$  translation. The  $C$  separation is constant at 3.5 Å and contour lines represent a change of  $E_{\text{int}} = 0.2 \text{ kcal mol}^{-1}$ . Black contours indicate where the disordermer pairs are equal in energy, blue indicates negative values (**3b** is more stable) and red indicates positive values (**3a** is more stable).

By taking the difference of the interaction terms for the entire dataset for **3a** from **3b**, in the vast majority of situations, **3b** possesses the stronger total SAPT0 interaction energy (Fig. 7). Table 1 provides points at which this difference in interaction energy is greatest, with **3b** being more stable than **3a** by around  $2 \text{ kcal mol}^{-1}$ . Comparison of the component energies at these coordinates reveals the largest difference in energy comes from the exchange term, as to be expected given its dominance in the total intermolecular interaction energy. The molecular arrangements at these points (see ESI†) suggest the more stacked arrangements of the thiophene moieties, including those with more S...S contact between the dimers, lie behind these increased exchange energies. A similar story unfolds when comparing **3a** and **3c**, though smaller differences are observed.

Using a similar procedure, the electronic couplings were calculated for each arrangement on the 3D map (Fig. 8). For brevity,

Table 1 Difference in SAPT0/jun-cc-pVDZ energies (in  $\text{kcal mol}^{-1}$ ) between disordermers **3b** and **3a** at selected  $A$ ,  $B$  coordinates (in Å), with more negative values indicating greater stabilization for **3b**.  $C$  displacement is constant at 3.5 Å

Displacement (Å)		$E^{3b} - E^{3a} (\text{kcal mol}^{-1})$				
$A$	$B$	$E_{\text{exch}}$	$E_{\text{elec}}$	$E_{\text{ind}}$	$E_{\text{disp}}$	$E_{\text{int}}$
3.00	0.75	−2.50	−0.19	−0.23	0.62	−2.29
3.00	3.00	−3.26	−0.30	0.17	1.26	−2.14
6.00	1.00	−3.17	0.07	0.14	0.76	−2.20
6.00	3.25	−4.00	0.26	0.39	1.09	−2.26

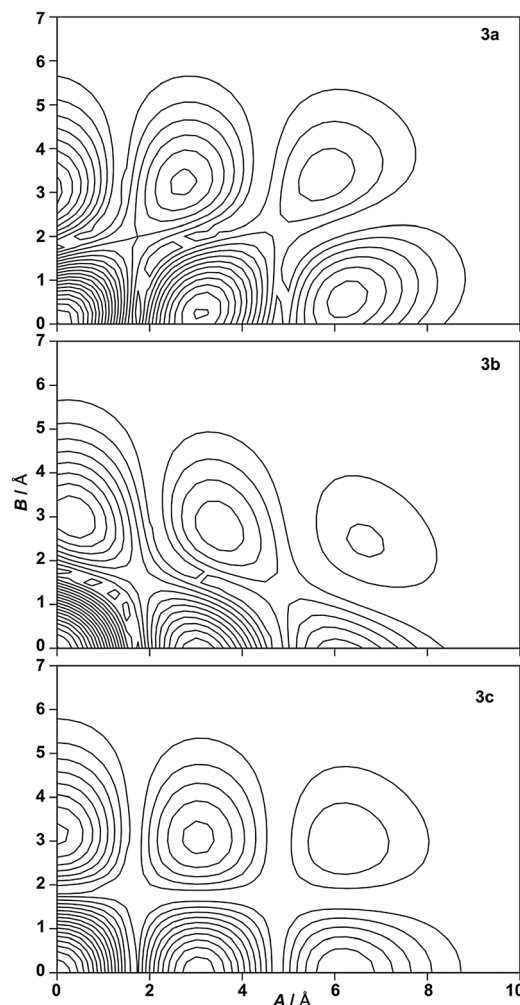


Fig. 8 Electronic couplings of disordermer pairs of *anti*-BDT (**3a**, **3b** and **3c**) as a function of  $A$  and  $B$  displacement as determined at the B3LYP/6-31G(d) level of theory.  $C$  displacement is constant at 3.5 Å and contour lines represent changes in electronic coupling of 0.02 eV.

we concentrate on  $t_h$ . The electronic couplings are, in general, largest for disordermer pair **3a** when compared to **3b** and **3c**, due to the heavy involvement of the sulfur atoms in the wave functions. Particular intermolecular displacements within a disordermer pair, however, can lead to larger electronic couplings.

### Long axis rotation: towards the herringbone structure

In addition to  $\pi$ -stacking, another common packing motif in organic semiconductor materials is the edge-to-face interaction of herringbone configurations. These can be modeled to a first approximation by the systematic rotation and concomitant shift in the  $C$ -direction of one molecule in the  $\pi$ -stacked pair. Here, we rotate one molecule about its long ( $A$ ) axis and shift it in the  $C$  direction by  $1.5 \times \sin(\theta)$ , in accordance with previous investigations of molecular rotation.<sup>28,29</sup> The issue of disorder is accounted for by rotation through a full  $360^\circ$  for the anthracene and *anti*- and *syn*-BDTs. Notably, BDT itself forms a herringbone packing structure<sup>39</sup> with an intermolecular angle of  $55^\circ$ . As the molecules in the crystal show translations in

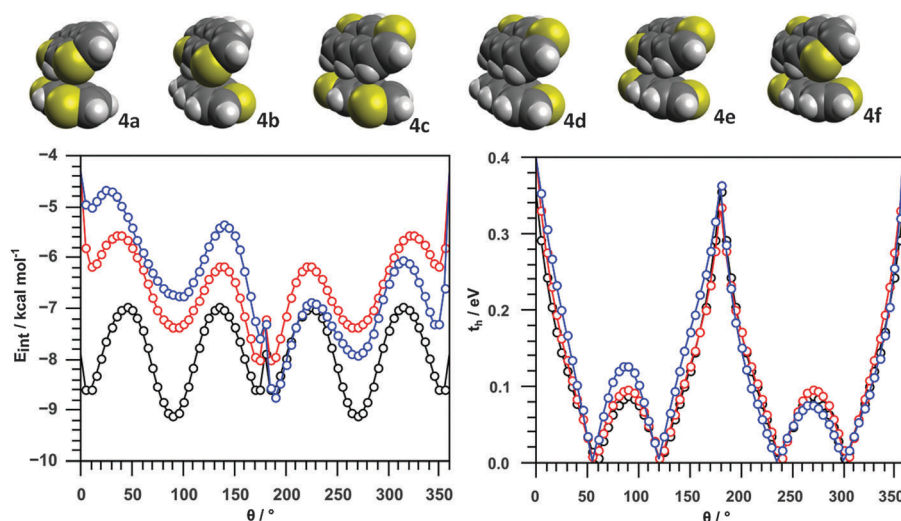


Fig. 9 Evolution of SAPT0/jun-cc-pVDZ interaction energy (left) and hole transfer integral, determined at the B3LYP/6-31G(d) level of theory, (right) of dimers of anthracene, *syn*-BDT and *anti*-BDT with rotation of one molecule in the pair.

multiple directions, direct comparison to the idealized results presented here are not trivial; there is no disorder of the thiophene rings in this reported crystal structure.

As a reference, the total SAPT0 interaction energy for an anthracene model dimer shows an approximate sinusoidal pattern, with constant peak amplitude, except for values close to 0 and 180° (Fig. 9). At these points, “ $\pi$ -stacking” leads to large dispersion interactions, though the increase in the repulsive exchange energy is even larger and results in a destabilized contact compared to those configurations that are slightly rotated. For *anti*-BDT, each of the waves between 0 and 180° show a different amplitude, with the sequence mirrored between 180 and 360° due to the molecular symmetry. *syn*-BDT exhibits smaller intermolecular interaction energies between the 0 and 180° rotation when compared to the *anti* isomer, though the interactions between *syn*-BDT isomers become more stabilizing when compared to *anti*-BDT beyond 180°.

Analysis of the individual SAPT0 components at different molecular rotations reveals the details of the edge-to-face interactions; to simplify the discussion, we consider only four rotation angles (see Table S1 in the ESI†). By analogy to the  $\pi$ -stacking investigations, we consider each of these as a 45° rotation, coupled with the disordermer concept of applying symmetry operations to one or more molecules. Thus, a rotation of 135° is the same as a rotation of 45° and a  $C_2(x)$  rotation of the bottom molecule (4b in Fig. 9). First we compare the simpler case of the *anti*-BDT: in 4e, two sulfur atoms (one coming from each BDT in the dimer) are in close contact on one side of the dimer (S...S), while a more C-H... $\pi$ -like interaction arises between the thiophene rings on the opposite side of the dimer. In 4f, the BDT arrangement leads to a combination of S... $\pi$  and C-H... $\pi$  interactions, with little-to-no S...S contact. 4f is the more energetically favorable configuration. The difference between the two disordermers comes from the electrostatic energy, most likely from the C-H... $\pi$  interaction: the proton bears a partial positive charge due to the polarization of the C-H bond, which can

therefore form a stabilizing electrostatic interaction with the negatively polarized  $\pi$  electron cloud. This interaction is further stabilized due to the close proximity of the edge proton to the electron rich sulfur atom in 4f.

*syn*-BDT can form four distinct molecular pairs due to the disorder. Of these, the weakest intermolecular interaction is found when the four sulfur atoms are in close proximity in 4a, a function of very large exchange repulsion.<sup>38</sup> Similarly the interaction in 4b is weakened by the large exchange energy related to the close contacts of the sulfur atoms. The strongest intermolecular interactions are found in disordermer pair 4c (followed by 4d), where the polarized C-H edge forms a strong electrostatic interaction with the  $\pi$  cloud around both electron rich sulfur atoms. Notably, the results of these differing sulfur-based edge-to-face interactions are consistent with recently reported desymmetrized silylethynyl ADTs that present completely different packing structures depending on the identity of the isomer.<sup>40</sup>

The electronic couplings, computed along the same rotational path, for anthracene and *anti*-BDT are similar at all rotational angles. *syn*-BDT shows stronger couplings than both anthracene and *anti*-BDT at rotation angles smaller than 180°, but weaker couplings at larger rotational angles; for *syn*-BDT, the sulfur atoms are involved in the intermolecular contact at small rotation angles, but not at the larger rotation angles, hence there is a direct (as expected) consequence of the geometric orientation on the electronic coupling. In contrast, *anti*-BDT consistently has one sulfur atom from each molecule involved in the intermolecular wave-function overlap, resulting in the electronic coupling between 0 and 180° being mirrored with further rotation through to 360°. Therefore the trend in electronic couplings with molecular rotation for BDT can be directly related to the orientation of the sulfur atoms in the dimer pairs.

With the above information that relates the intermolecular interactions and electronic couplings among disordered molecular pairs in BDT, one can begin to identify how the presence



and placement of the sulfur atoms in ADT define the preferred molecular orientations and resulting electronic interactions. Taking a closer look at the previously reported isomerically pure anthradithiophene crystal structures,<sup>20–23</sup> the dominant disorderers tend to minimize the sulfur contacts with nearest neighbors. In each of these studies, it is the *anti* isomer that forms the more ordered packing structure: the *anti* isomer is able to sustain a pattern of forming the strongest possible intermolecular interactions, minimizing sulfur contacts, in the solid state. In contrast, if a *syn* isomer attempts to form configurations with sulfur-free interactions with a neighbor molecule, the contacts with the next neighbor must necessarily involve sulfur atoms, and therefore be weaker due to increased exchange repulsion. It is this attempt to minimize the exchange repulsion and induce more stable intermolecular interactions that explains key aspects of the difference in the degrees of disorder in the relative isomers in ADT. It is not clear, however, whether disordered molecules occur randomly through the bulk material or form in domains, either of which would have an impact on charge-carrier transport of the material. The electronic coupling in the more ordered *anti* isomer is expected to be more consistent, with similar coupling between adjacent molecules throughout the bulk. In contrast, the electronic couplings in the *syn* isomers can be larger due to the increased sulfur contacts, but less uniform due to the increased disorder. This variation in electronic coupling might generate local trapping sites, reducing the charge-carrier mobilities in the *syn* isomers, a phenomenon described in recent publications.<sup>20,21</sup>

## Conclusions

The chemistry used in the design of organic semiconductors is vast. By considering the role of molecular isomerism in BDT, along with packing isomerism due to disorder in the solid state, we introduced the concept of the disordermer, which can play a defining role in the intrinsic characteristics of organic semiconductors. By constructing dimers for two BDT isomers and varying four parameters –  $\pi$ -stacking distance, long- and short-axis translation, and molecular rotation – we developed a map of some of the possible intermolecular interactions that may be found in thienoacenes and their subsequent impact on the electronic couplings. Through these investigations, we found that contacts where sulfur atoms are in close proximity are generally less stable; the exception is the edge-to-face (herringbone) interaction of the positively polarized C–H edge interacting directly with the electron-rich  $\pi$  cloud around the sulfur atoms on the neighboring molecule. In contrast, the electronic couplings tend to be larger when direct sulfur contacts are involved.

An important outcome of this work is that the substitution pattern of sulfur atoms in thienoacenes can impact the amount of disorder expected in crystalline structures. In a number of published reports on isomerically pure thienoacenes, the *anti* isomer forms more ordered structures, which can be explained by the ability of this isomer to form a large network of the more energetically favorable interactions described above. The *anti*

isomer also usually performs better in transistor devices, which might be explained by the increased molecular order that can bring with it a more consistent pathway for charge-carrier transport due to more uniform electronic couplings between neighboring molecules. While this work only takes into account the influence of sulfur as a possible heteroatom substitution, and neglects the influence of the alkyl substituents that are often used to develop solution-processable molecular materials, we are beginning to develop an important foundation for providing a deeper quantum-chemical picture of how chemical substitution in the  $\pi$ -conjugated backbone can be used as means to control molecular packing and the resulting material electronic properties.

## Acknowledgements

This work was supported in part by seed funds from the Center for Applied Energy Research (CAER) at the University of Kentucky. C. R. thanks the University of Kentucky Vice President for Research for start-up funds. The authors thank Sean R. Parkin and John E. Anthony, Department of Chemistry, University of Kentucky, for helpful discussions. JEA and KJT thank the National Science Foundation (CMMI-1255494) for partial support of this research.

## References

- 1 C. Sutton, C. Risko and J.-L. Brédas, *Chem. Mater.*, 2016, **28**, 3–16.
- 2 U. H. F. Bunz, *Chem. – Eur. J.*, 2009, **15**, 6780–6789.
- 3 K. Takimiya, Y. Kunugi, Y. Konda, N. Niihara and T. Otsubo, *J. Am. Chem. Soc.*, 2004, **126**, 5084–5085.
- 4 K. Takimiya, S. Shinamura, I. Osaka and E. Miyazaki, *Adv. Mater.*, 2011, **23**, 4347–4370.
- 5 M. M. Payne, S. A. Odom, S. R. Parkin and J. E. Anthony, *Org. Lett.*, 2004, **6**, 3325–3328.
- 6 J.-I. Park, J. W. Chung, J.-Y. Kim, J. Lee, J. Y. Jung, B. Koo, B.-L. Lee, S. W. Lee, Y. W. Jin and S. Y. Lee, *J. Am. Chem. Soc.*, 2012, **137**, 12175–12178.
- 7 K. Yamaguchi, S. Takamiya, M. Minami, Y. Doge, Y. Nishide, H. Osuga, K. Uno and I. Tanaka, *Appl. Phys. Lett.*, 2008, **93**, 043302.
- 8 N. Wang, Z. Chen, W. Wei and Z. Jiang, *J. Am. Chem. Soc.*, 2013, **135**, 17060–17068.
- 9 C. Cabanetos, A. El Labban, J. A. Bartelt, J. D. Douglas, W. R. Mateker, J. M. J. Fréchet, M. D. McGehee and P. M. Beaujuge, *J. Am. Chem. Soc.*, 2013, **135**, 4656–4659.
- 10 M. Zhang, Y. Gu, X. Guo, F. Liu, S. Zhang, L. Huo, T. P. Russell and J. Hou, *Adv. Mater.*, 2013, **25**, 4944–4949.
- 11 L. Huo and J. Hou, *Polym. Chem.*, 2011, **2**, 2453.
- 12 J. E. Anthony, *Chem. Rev.*, 2006, **106**, 5028–5048.
- 13 O. D. Jurchescu, S. Subramanian, R. J. Kline, S. D. Hudson, J. E. Anthony, T. N. Jackson and D. J. Gundlach, *Chem. Mater.*, 2008, **20**, 6733–6737.
- 14 H. Ebata, T. Izawa, E. Miyazaki, K. Takimiya, M. Ikeda, H. Kuwabara and T. Yui, *J. Am. Chem. Soc.*, 2007, **129**, 15732–15733.



- 15 H. Minemawari, T. Yamada, H. Matsui, J. Tsutsumi, S. Haas, R. Chiba, R. Kumai and T. Hasegawa, *Nature*, 2011, **475**, 364–367.
- 16 S. E. Wheeler and J. W. G. Bloom, *J. Phys. Chem. A*, 2014, **118**, 6133–6147.
- 17 E. G. Hohenstein and C. D. Sherrill, *J. Phys. Chem. A*, 2009, **113**, 878–886.
- 18 E. G. Hohenstein, J. Duan and C. D. Sherrill, *J. Am. Chem. Soc.*, 2011, **133**, 13244–13247.
- 19 S. Tsuzuki, K. Honda and R. Azumi, *J. Am. Chem. Soc.*, 2002, **124**, 12200–12209.
- 20 D. Lehnher, A. R. Waterloo, K. P. Goetz, M. M. Payne, F. Hampel, J. E. Anthony, O. D. Jurchescu and R. R. Tykwinski, *Org. Lett.*, 2012, **14**, 3660–3663.
- 21 R. K. Hallani, K. J. Thorley, Y. Mei, S. R. Parkin, O. D. Jurchescu and J. E. Anthony, *Adv. Funct. Mater.*, 2015, DOI: 10.1002/adfm.201502440.
- 22 M. Mamada, T. Minamiki, H. Katagiri and S. Tokito, *Org. Lett.*, 2012, **14**, 4062–4065.
- 23 M. Mamada, H. Katagiri, M. Mizukami, K. Honda, T. Minamiki, R. Teraoka, T. Uemura and S. Tokito, *ACS Appl. Mater. Interfaces*, 2013, **5**, 9670–9677.
- 24 A. Cammers and S. Parkin, *CrystEngComm*, 2004, **6**, 168.
- 25 A. D. Becke, *J. Chem. Phys.*, 1993, **98**, 5648.
- 26 W. J. Hehre, *J. Chem. Phys.*, 1972, **56**, 2257.
- 27 M. J. Frisch, *et al.*, *Gaussian 09, Revision A.02*, 2009.
- 28 E. F. Valeev, V. Coropceanu, D. A. da Silva Filho, S. Salman and J.-L. Brédas, *J. Am. Chem. Soc.*, 2006, **128**, 9882–9886.
- 29 K. J. Thorley and C. Risko, *J. Mater. Chem.*, 2015, DOI: 10.1039/C5TC03765D.
- 30 E. G. Hohenstein, R. M. Parrish, C. D. Sherrill, J. M. Turney and H. F. Schaefer, *J. Chem. Phys.*, 2011, **135**, 174107.
- 31 E. G. Hohenstein and C. D. Sherrill, *J. Chem. Phys.*, 2010, **132**, 184111.
- 32 R. A. Kendall, T. H. Dunning and R. J. Harrison, *J. Chem. Phys.*, 1992, **96**, 6796.
- 33 E. Papajak, J. Zheng, X. Xu, H. R. Leverentz and D. G. Truhlar, *J. Chem. Theory Comput.*, 2011, **7**, 3027–3034.
- 34 J. M. Turney, A. C. Simmonett, R. M. Parrish, E. G. Hohenstein, F. A. Evangelista, J. T. Fermann, B. J. Mintz, L. A. Burns, J. J. Wilke, M. L. Abrams, N. J. Russ, M. L. Leininger, C. L. Janssen, E. T. Seidl, W. D. Allen, H. F. Schaefer, R. A. King, E. F. Valeev, C. D. Sherrill and T. D. Crawford, *Wiley Interdiscip. Rev.: Comput. Mol. Sci.*, 2012, **2**, 556–565.
- 35 M. S. Marshall, L. A. Burns and C. D. Sherrill, *J. Chem. Phys.*, 2011, **135**, 194102.
- 36 C. Sutton, M. S. Marshall, C. D. Sherrill, C. Risko and J.-L. Brédas, *J. Am. Chem. Soc.*, 2015, **137**, 8775–8782.
- 37 J. L. Brédas, J. P. Calbert, D. A. da Silva Filho and J. Cornil, *Proc. Natl. Acad. Sci. U. S. A.*, 2002, **99**, 5804–5809.
- 38 See ESI† for further details.
- 39 K. Takimiya, Y. Konda, H. Ebata, N. Niihara and T. Otsubo, *J. Org. Chem.*, 2005, **70**, 10569–10571.
- 40 R. K. Hallani, K. J. Thorley, A. K. Hailey, S. R. Parkin, Y.-L. zLoo and J. E. Anthony, *J. Mater. Chem. C*, 2015, **3**, 8956–8962.